Available online at www.sciencedirect.com
SCIENCE DIRECT®
Journal of Nuclear Materials 337–339 (2005) 691–696
journal of nuclear materials
www.elsevier.com/locate/jnucmat

Suppression of large edge localized modes in high confinement DIII-D plasmas with a stochastic magnetic boundary

T.E. Evans [a,*], R.A. Moyer [b], J.G. Watkins [c], P.R. Thomas [d], T.H. Osborne [a], J.A. Boedo [b], M.E. Fenstermacher [e], K.H. Finken [f], R.J. Groebner [a], M. Groth [e], J. Harris [g], G.L. Jackson [a], R.J. La Haye [a], C.J. Lasnier [e], M.J. Schaffer [a], G. Wang [h], L. Zeng [h]

[a] *General Atomics, P.O. Box 85608, San Diego, CA 92186-5608, USA*
[b] *University of California at San Diego, La Jolla, CA 92093-0417, USA*
[c] *Sandia National Laboratories, Albuquerque, NM 87185-1129, USA*
[d] *Association Euratom-CEA, CEA Cadarache, F-13108, St. Paul-lez-Durance, France*
[e] *Lawrence Livermore National Laborabory, Livermore, CA 94550, USA*
[f] *Forschungszentrum Jülich, Institute for Plasma Physics, D52425 Jülich, Germany*
[g] *Australian National University, Canberra, Australia*
[h] *University of California, Los Angeles, California, USA*

Abstract

Large 70 Hz Type-I edge localized modes (ELMs) are converted into small 130 Hz oscillations using edge resonant magnetic perturbations (RMPs) from a coil with currents $\leqslant 0.4\%$ I_p in double null DIII-D plasmas. When the RMP is properly phased with respect to the background field errors, all but a few isolated ELM-like events are suppressed. The impulsive pedestal energy loss $\Delta E_{ELM}/\Delta t^{1/2}$ to the scrape-of layer is reduced a factor of $\geqslant 20$ relative to the Type-I ELMs and the core confinement is unaffected by the perturbation field. Significant changes in the properties of the ELMs are also observed when edge RMPs are applied to lower single null plasmas but the nature of these changes are much more complex. Both lower single null and double null plasmas are being studied to determine how ELM control techniques based on the application of edge RMPs can be expected to scale to future devices such as ITER.

PACS: 28.52.−s; 52.55.Fa; 52.55.Rk; 52.55.−s
Keywords: ELM control; Edge pedestal; Stochastic boundary; DIII-D; Divertor

1. Introduction

Efficient fusion power production with a tokamak confinement system relies on maintaining good core confinement, low impurity concentrations and good magnetohydrodynamic (MHD) stability. Because of the relative stiffness of the core transport, large pressure

* Corresponding author.
E-mail address: evans@fusion.gat.com (T.E. Evans).

0022-3115/$ - see front matter © 2004 Elsevier B.V. All rights reserved.
doi:10.1016/j.jnucmat.2004.10.062

gradients are needed across the pedestal region to obtain pedestal heights sufficient for achieving burning plasmas in the International Thermonuclear Experimental Reactor (ITER) [1]. Predictions for ITER suggest that a temperature pedestal of approximately 4–5 keV is needed to achieve a fusion power gain $Q \geqslant 10$. However, the associated large pedestal gradients are known to drive instabilities such as edge localized modes (ELMs). Scaling the energy dump due to these ELMs from current tokamaks like DIII-D to ITER [1–4] implies that carbon divertor tiles will significantly exceed their $45\,\mathrm{MJ\,m^{-2}\,s^{-1/2}}$ [5] ablation threshold limit during each Type-I ELM impulse.

Because of their potential for damaging divertor target plates in high confinement discharges, ELMs must be controlled in future burning plasma devices such as ITER. The control method used must be capable of reducing the amplitude of ELM energy impulses without significantly altering the height of the pedestal. It must also be capable of replacing the impulsive particle transport (thermal electrons and deuterium as well as impurity ions) driven by the ELMs with a more benign transport mechanism (i.e., a lower amplitude, longer duration transport process) in order to avoid an uncontrolled increase in the core density or a detrimental accumulation of the impurity ions in the core plasma. Several types of steady-state relevant control techniques have been explored with varying degrees of success. These include pedestal impurity seeding [6], the injection of small pellets to trigger ELM-like events [7] and the use of resonant magnetic perturbations (RMPs) [8–10]. In this paper we focus on recent results using RMPs in DIII-D.

2. Experimental background and results

A variety of small, $10^{-5} \leqslant \delta B/B_\phi \leqslant 10^{-3}$, but significant non-axisymmetric magnetic perturbation sources are common to all tokamaks. These include: fields from MHD control coils such as the DIII-D I-coil [11] and from locked mode corrections coils such as the DIII-D C-coil [12], so-called field errors caused by multi-millimeter shifts or distortions in several of the poloidal, shaping, ohmic or diveror field coils [13], stray fields due to currents in radial feeders or bus bars and millimeter scale ensemble randomness built-in to the toroidal and poloidal field coil sets due to unbalanced operational forces and the buildup of engineering tolerances known as intrinsic topological noise [14].

Studies of the effects of these perturbations in circular limited and poloidally diverted plasma with field line integration and mapping codes show that they create field line resonances which result in complex topological structures such as helical islands surrounded by separatrices that split into pairs of intersecting invariant manifolds. These intersecting invariant manifolds form elaborate webs, known in non-linear dynamical systems theory as homoclinic tangles [15], that are responsible for stochastic mixing of the field lines. An interesting variety of homoclinic tangles has recently been shown to exist in the primary separatrix of a poloidally diverted tokamak and is believed to be the mechanism by which field lines are transported from inside the separatrix into the scrape-off layer (SOL) [16]. In addition, detailed field line integration studies of the magnetic topology in the DIII-D pedestal, with various shapes and q (safety factor) profiles, show that poloidally diverted tokamaks are much more sensitive to the onset of global stochasticity and the loss of magnetic flux than circular limited plasmas due to the high edge magnetic shear [17].

A significant requirement for interpreting the results of any magnetic perturbation experiment on a particular tokamak is first to develop a good understanding of all the intrinsic perturbation sources on that machine. Elaborate, one-of-a-kind measurements of the non-axisymmetric field errors in DIII-D indicate that although these sources are relatively small, averaging to $\sim$1 G for the $n = 1$ component on a circle near the major axis, they have a substantial impact on the performance of the machine [13]. This fact has been well established by results from a variety of MHD stability and locked mode experiments [12,18].

The resistive wall mode (RWM) control coil mounted inside the DIII-D vacuum vessel, referred to as the I-coil [11], is used as a controlled perturbation field source for the ELM suppression experiments discussed in this paper. The 3D geometry of the I-coil is shown in Fig. 1. Since the C-coil, used to correct measured field errors on the $m,n = 2,1$ surface, is known to perturb both the core and pedestal plasma [19] it was turned off for the double-null (DN) discharges discussed in this paper but was required during the lower single-null (LSN) discharges to avoid locked modes.

In order to minimize core RMPs due to the I-coil, toroidally adjacent segments are driven with opposite

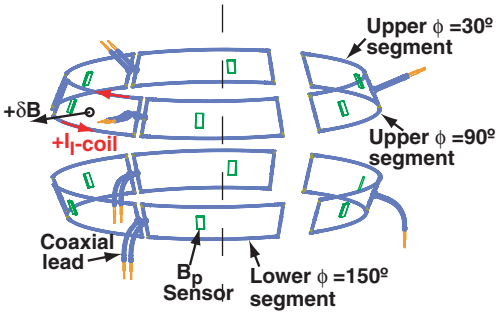

Fig. 1. The DIII-D I-coil is comprised of six segments above the equatorial plane (upper) and six segments below the equatorial plane (lower) centered at 60° toroidal angle (ϕ) increments (starting at 30°) inside the DIII-D vacuum vessel.

polarities producing an $n = 3$ toroidal mode structure. The geometry of the I-coil produces $m = 12 \pm 3$ modes that are compatible with edge resonant studies. Positive current is defined to be in the counter-clockwise direction as viewed inward toward the toroidal axis and the corresponding perturbation field (δB) points in the direction of positive major radius R (see the upper segment at $\phi = 210°$ in Fig. 1). The up/down parity of the coil is referred to as 'even' when the upper and lower coil segments have the same polarity at each toroidal angle ϕ and 'odd' when these polarities are opposite. The toroidal phase angle of the I-coil perturbation $\phi_{\text{I-coil}}$ is two-fold symmetric where $\phi_{\text{I-coil}} = 0°$ is defined as the configuration where the current in the upper $\phi = 30°$ segment is positive and $\phi_{\text{I-coil}} = 60°$ has negative current in the upper $\phi = 30°$ segment. Each segment is limited to a maximum current of 5 kA.

Both DN and LSN discharges were used during the experiments discussed in this paper. Fig. 2(a) shows the DN flux surface shape and Fig. 2(b) shows the LSN shape while Fig. 2(c) shows the ITER scenario two shape (scaled down by a factor of 3.7 to fit in the DIII-D vacuum vessel) for comparison. We see from Fig. 2 that the ITER shape lies roughly between the two DIII-D shapes. The DN discharge has an elongation (κ) of 1.8 with upper (δ_{up}) and lower (δ_{low}) triangularities of 0.35 and 0.73 respectively, a toroidal magnetic field $B_{\text{T}} = 1.6$ T, a plasma current $I_{\text{p}} = 1.1$ MA, a neutral beam heating power $P_{\text{NBI}} = 5.1$ MW and is biased downward by 2 cm. In this discharge, the line averaged electron density (n_{e}) is $7.2 \times 10^{19}\,\text{m}^{-3}$ with $\beta_{\text{N}} = 2.2$, $H_{\text{L89}} = 2.1$ and a safety factor at the 95% flux surface (q_{95}) of 3.7. The time evolution of I_{p}, P_{NBI}, n_{e}, the D_2 gas fueling and the I-coil pulse ($I_{\text{coil}} = 4.4$ kA) for DN discharge 115467 is shown in Fig. 3 along with a representative lower divertor D_α signal. The LSN discharge (117823) had the following parameters: $B_{\text{T}} = 1.9$ T,

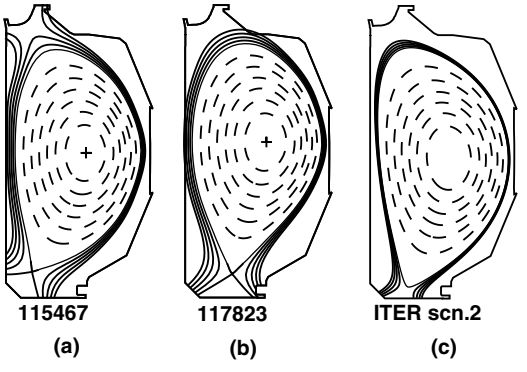

Fig. 2. Comparison between DIII-D shapes for discharges: (a) 115467:DN and (b) 117823:LSN that were used for ELM suppression studies. A scaled down view of the ITER scenario 2 shape (c) is also shown.

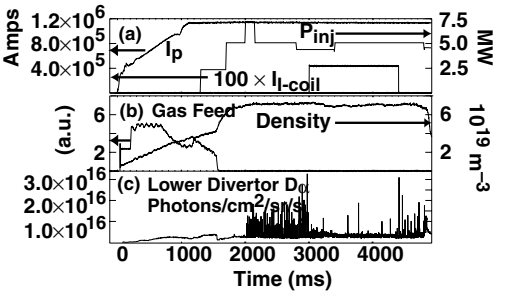

Fig. 3. Temporal evolution of: (a) I_{p}, P_{inj}, the $I_{\text{I-coil}}$ current, (b) the D_2 gas fueling, n_{e} and (c) a lower divertor D_α signal in DN discharge 115467.

$I_{\text{p}} = 1.1$–1.4 MA, $n_{\text{e}} = 4.0$–$4.8 \times 10^{19}\,\text{m}^{-3}$, $\kappa = 1.8$, $\delta_{\text{low}} = 0.38$, $P_{\text{NBI}} = 13.1$ MW, $\beta_{\text{N}} = 2.4$, $H_{\text{L89}} = 1.8$, $3.3 \leqslant q_{95} \leqslant 3.9$ and its time evolution is shown in Fig. 4.

First we describe the DN plasma response to the odd parity, $\phi_{\text{I-coil}} = 0°$, I-coil pulse shown in Fig. 3(a). In this case, the dynamical state of the pedestal plasma changes significantly and large Type-I ELMs are almost entirely eliminated except for a few randomly interspersed ELM-like spikes. This suppression takes place within a single ELM cycle (~12 ms) and is seen globally on all of the ELM diagnostics toroidally and poloidally distributed around the machine as shown in Fig. 5(a)–(i). The nature of the changes seen in the pedestal dynamics is best displayed by focusing on narrower time windows before and during the I-coil pulse. Fig. 6 shows two 11 ms windows, one without the I-coil pulse, Fig. 6(a), showing the evolution of a single 70 Hz Type-I ELM and one during the I-coil pulse, Fig. 6(b), showing a 2 ms quiet phase followed by a 6 ms active phase that characterize the small 130 Hz oscillations induced by the I-coil RMP. These oscillations correspond to a small, ~1–2 mm, global expansion of the outer flux surfaces during the quiet phase and an equivalent contraction during the active phase. This behavior is similar to a ~3 mm contraction seen during a Type-I crash which is followed an

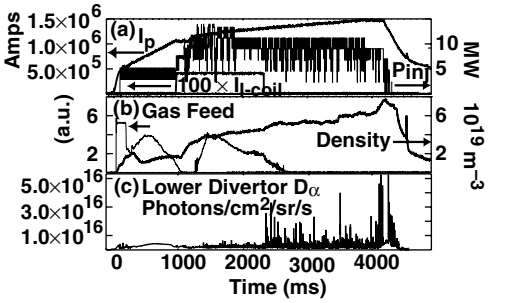

Fig. 4. Temporal evolution of: (a) I_{p}, P_{inj}, the $I_{\text{I-coil}}$ current, (b) the D_2 gas fueling, n_{e} and (c) a lower divertor D_α signal in LSN discharge 117823.

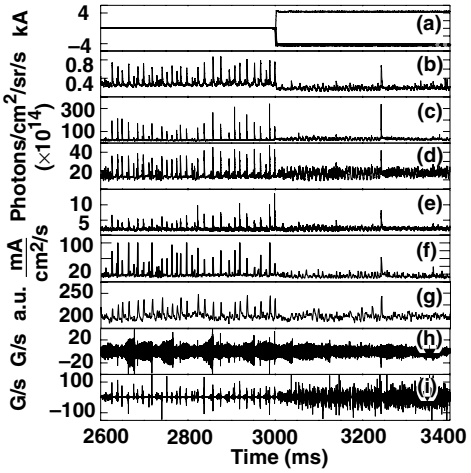

Fig. 5. Type-I ELM suppression in DN discharge 115467 during the: (a) $I_{\text{I-coil}}$ current pulse (in the upper and lower 30° segments) on the, (b) midplane D_α at $\phi = 45°$, (c) lower divertor D_α at $\phi = 150°$, (d) upper divertor D_α at $\phi = 150°$, (e) inner wall D_α at $\phi = 135°$, (f) lower divertor ion saturation current at $\phi = 180°$, (g) IRTV surface temperature at $\phi = 165°$, (h) core B_{dot} at the outer midplane $\phi = 322°$ probe, and (c) edge B_{dot} at divertor $\phi = 322°$ probe.

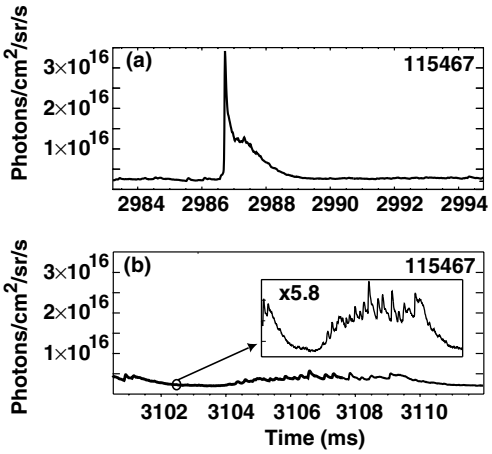

Fig. 6. An enlargement of a Type-I ELM (a) using the D_α signal shown in Fig. 5(c), and (b) one cycle of a D_α oscillation during the I-coil phase. The inset shows the detailed features of these oscillations on an expanded scale (×5.8).

expansion as the profile recovers. The energy lost from the pedestal during a typical Type-I ELM contraction in this discharge is approximately 25 ± 10 kJ as shown by the solid line in Fig. 7(a). This energy is lost within the first 200 μs of the crash resulting in an impulse source of 1.1×10^6 J/s$^{1/2}$. During the I-coil pulse, it is difficult to resolve the small changes that take place in the pedestal energy content. The drops observed are typically about 5–15 kJ or less. These drops also evolve slowly during

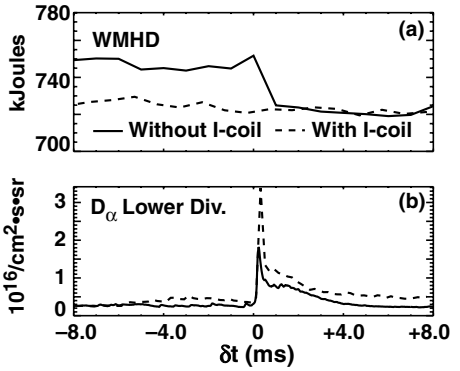

Fig. 7. (a) The stored energy (WMHD) computed from a fast (500 μs resolution) equilibrium reconstruction showing a change associated with an ELM (solid line) and no significant change during the isolated ELM-like event at 3243 ms in Fig. 5. The lower divertor D_α (100 μs resolution) behavior for an ELM (solid line) and the isolated event (dashed line) are shown in (b) relative to the onset time of the two events.

the active phase of the oscillation cycle resulting in a maximum impulse source of no more than 4.5×10^4 J/s$^{1/2}$ or a factor of 24 reduction compared to the Type-I ELM impulses. A significant reduction in the ELM induced divertor heat flux as measure by a fast infrared camera (IR) is also seen during the ELM suppression phase with the I-coil energized. Fig. 8(a) shows a radial profile of the heat flux across the lower divertor surface averaged over five Type-I ELMs just before the I-coil pulse. These profiles are taken at times corresponding to the peak heat flux loading due to each ELM. Fig. 8(b) shows a radial profile of the heat flux distribution across the lower divertor surface averaged over four time slices during the active phase of the oscillations shown in Fig. 6(b) with the I-coil is energized. We see that the heat flux due to the ELMs is reduced to the noise level of the fast IR camera during the I-coil

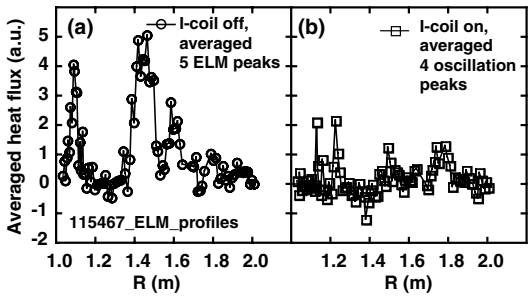

Fig. 8. Fast infrared camera data showing a radial profile ($\Delta t = 101$ μs per profile) of the lower divertor heat flux: (a) averaged over five Type-I ELM peaks just prior to the I-coil pulse and (b) averaged over four of the small oscillations peaks seen during the *I*-coil pulse.

pulse (i.e., at least a factor of five reduction in the largest peaks during the suppression phase compared to the ELMing phase just prior to the I-coil pulse).

As seen in Fig. 3, some large spikes do remain in the D_α signals that resemble ELMs. These events increase the surface temperature of the divertor target plates [Fig. 5(g)] and the incident particle flux [Fig. 5(f)] but they do not appear to be connected with a loss of stored energy from the core or pedestal plasma usually seen during Type-I ELMs as shown in Fig. 7(a). In addition, radially resolved soft X-ray data shows that the event at 3243 ms in Fig. 5 starts near the $q = 3/2$ surface and is not correlated with a sawtooth crash. Based on the limited data available at this time we can not be certain if these events are intermittent Type-I ELMs or some instability located deeper inside the core plasma (e.g. an internal magnetic reconnection process) that drive energetic particles into the scrape-off layer.

Large Type-I ELMs are also significantly modified in pumped LSN discharges at lower densities than in the DN discharge discussed above. In this case, the pedestal response to an $n = 3$, odd parity, I-coil pulse with $\phi_{\text{I-coil}} = 0°$ toroidal phasing is rather different than in the DN discharge. Although the effect of the I-coil on the ELMs is seen on all the D_α recycling signals, it is most pronounced in the lower divertor private flux region. For example, Fig. 9 shows how the ELMs change near the center of the private flux region in discharge 117 823 (see Figs. 2(b) and 4 for a summary of the discharge parameters). Here, the I-coil pulse is switched on at about the same time as the L–H transition and switched off at $t = 2415$ ms. The small 130 Hz features seen during the I-coil pulse in Fig. 9(b) have a compound structure compared to the large Type-I ELMs that appear following the I-coil pulse but are approximately an order of magnitude lower in amplitude and a factor of two higher in frequency. Although they appear to be similar in some respects to Type-II ELMs a more detailed analysis in needed to confirm this possibility. Note that the D_2 gas fueling valve was commanded to come on during the I-coil pulse, as shown in Fig. 4(b), which was not the case during the DN ELM suppression discharges [Fig. 3(b)]. This increases the recycling in the SOL and affects the behavior of the ELMs near the strike points differently than those in the private flux region. Also note that the continuous n_e rise during the discharge is typical of plasmas with increasing I_p and is relatively unaffected by the additional D_2 gas fueling or the I-coil pulse.

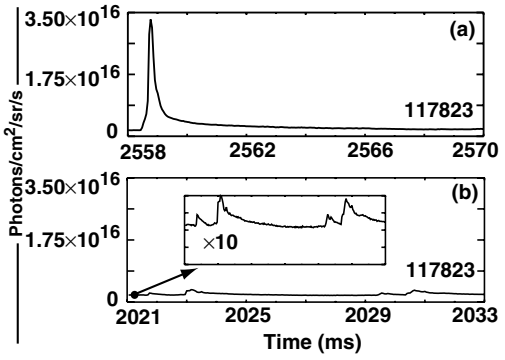

Fig. 9. An enlargement of a Type-I ELM (a) using the D_α signal shown in Fig. 4(c) and (b) an equivalent time window showing the D_α behavior during the I-coil pulse. The inset shows how the structure of the ELMs are changed on an expanded scale (×10).

3. Discussion

The affects of field errors on poloidal and toroidal energy loading asymmetries were first studied in ASDEX [20] where it was suggested that external perturbation coils could be used to control asymmetries in the divertors and to modify boundary layer processes such as ELMs and L–H transition dynamics. Subsequently, experiments were carried out on JFT-2 M [8] and Compass [9], with $n = 1$ RMP coils, showing that ELM-free H-modes could be converted into ELMing H-modes with small, high frequency, Type-III ELMs. Although the confinement associated with Type-III ELMing regimes is typically inferior to that in Type-I ELMing regimes, these initial experiments confirmed the idea that small RMPs have a significant impact on the dynamic of the pedestal. The experiments discussed in this paper show that it is possible, with the proper external coil design and discharge shape, to suppress large Type-I ELMs without degrading (or overly enhancing) the quality of the confinement. The demonstration of a broad operating window for ELM suppression using RMPs would be of considerable importance for burning plasma devices such as ITER.

The best ELM suppression found to date (Fig. 5) using the $n = 3$ I-coil configurations is obtained in DN discharges biased downward by about 2 cm. In this case, the effectiveness of the perturbation is particularly sensitive to changes in the plasma shape and q_{95} with the strongest ELM suppression found between $3.5 \leqslant q_{95} \leqslant 4.0$. The parity and toroidal phase of the I-coil pulse also have significant effects on the pedestal response. Odd parity pulses with $\phi_{\text{I-coil}} = 0°$ toroidal phasing has the largest effect while odd parity, $\phi_{\text{I-coil}} = 60°$, pulses produce smaller changes in the ELMs and higher midplane recycling with flatter T_e profile in the outer pedestal region. The $\phi_{\text{I-coil}} = 60°$ odd parity response looks remarkably similar to that seen during stochastic magnetic boundary experiments in low power circular tokamaks [21] and indicates the presence of a background non-axisymmetric perturbation source (such as field errors) that mix differently with the applied RMP

in the two toroidal phases used [10]. Even parity $\phi_{\text{I-coil}} = 0°$ I-coil pulses are less effective for suppressing ELMs and produce 190 Hz oscillations in all D_α signals that are typically larger than Type-I ELMs in the mid-plane D_α signals.

It is interesting to note that in DN discharges a reduction in the odd parity $\phi_{\text{I-coil}} = 0°$ I-coil current from 4.4 to 2.2 kA reduces the frequency of the Type-I ELMS from 70 Hz to 45 Hz for the first 300 ms with no change in the amplitude followed by period of relatively good ELM suppression (the ELMs are almost entirely eliminated except for a few isolated ELM-like events) for the remainder of the pulse. Additionally, the average peak heat flux to the lower divertor target, integrated over 16.6 ms, drops by 21% with $I_{\text{I-coil}} = 2.2$ kA and 47% with $I_{\text{I-coil}} = 4.4$ kA compared to a case without the I-coil while spreading out radially from 0.04 m FWHM to 0.12 m with the 4.4 kA RMP. It is also noted that in DN discharges, identical to those discussed above which remain in an L-mode at lower NBI power levels, no measurable change is observed during I-coil pulses implying that the plasma response to the RMP is amplified in high confinement regimes.

In LSN discharges $\phi_{\text{I-coil}} = 0°$ odd parity I-coil pulses reduce the amplitude of D_α bursts from Type-I ELMs in the private flux region by an order of magnitude and increase their frequency by a factor of two. Although the modifications seen in the ELMs are global, significant poloidal variations in the characteristics of the remaining ELMs are also observed during the I-coil pulse in this case.

4. Conclusions

Large Type-I ELMs have been suppressed, except for a few isolated events, with $n = 3$ edge resonant magnetic perturbations in DN discharges and significantly modified in LSN discharges without altering the core confinement. The effectiveness of the suppression depends on the plasma shape, q_{95} and the way the coils are configured (i.e., the up-down parity or poloidal mode spectrum and the toroidal phase of the perturbation relative to existing field errors). Both the impulsive and peak steady state heat flux to the divertor target plates are substantially reduced during the I-coil pulse.

These results suggest that relatively simple perturbation coils may be useful for controlling ELMs in next-step burning plasmas devices such as ITER.

Acknowledgments

Work supported by the US Department of Energy under DE-FC02-04ER54698, DE-AC04-94AL85000, W-7405-ENG-48, DE-FG02-04ER54758, DE-FG03-01ER54615, DE-FG02-89ER53297, and DE-FG03-01ER54615.

References

[1] H.D. Pacher, ITER Design Description Document ITER No. G 17 DDD 1 96-08-21 W2.1 Appendix E9, Section 1.7, 1996.
[2] A. Loarte et al., Plasma Phys. Control. Fusion 44 (2002) 1815;
A. Loarte et al., Plasma Phys. Control. Fusion 45 (2003) 1549.
[3] A.W. Leonard et al., Plasma Phys. Control. Fusion 44 (2002) 945.
[4] M.E. Fenstermacher et al., Plasma Phys. Control. Fusion 45 (2003) 1597.
[5] G. Federici et al., J. Nucl. Mater. 313–316 (2003) 11;
G. Fedrici et al., Plasma Phys. Control. Fusion 45 (2003) 1523.
[6] G.P. Maddison et al., Plasma Phys. Control. Fusion 45 (2003) 1657.
[7] P.T. Lang et al., Nucl. Fusion 43 (2003) 1110.
[8] H. Tamai et al., J. Nucl. Mater. 220–222 (1994) 365.
[9] S.J. Fielding et al., in: Proceedings of 28th EPS Conference on Controlled Fusion and Plasma Physics, Maderia, Portugal, 2001, Vol. 25A, European Physical Society, 2002, p. 1825.
[10] T.E. Evans et al., Phys. Rev. Lett. 92 (2004) 235003-1.
[11] G.L. Jackson et al., in: Proceedings of 30th EPS Conference on Controlled Fusion and Plasma Physics, St. Petersburg, Russia, 2003, P-4.47 on CD-ROM.
[12] J.T. Scoville, R.J. La Haye, in: Proceedings of 14th IEE/NPSS Symposium on Fusion Engineering, San Diego 1991, Vol. II, Institute of Electrical and Electronics Engineers, Inc. Piscataway, 1992, p. 1144.
[13] J.L. Luxon et al., Nucl. Fusion 43 (2003) 1813.
[14] T.E. Evans, in: Proceedings of 18th European Conference on Controlled Fusion and Plasma Physics, Berlin, Germany, 1991, Part II, European Physical Society, Petit-Lancy, 1991, p. 65.
[15] J. Guckenheimer, P. Holmes, Nonlinear oscillations, dynamical systems, and bifurcations of vector fields, in: Applied Mathematical Science, Vol. 42, Springer-Verlag, New York, 1983, p. 45.
[16] R.K.W. Roeder, B.I. Rapoport, T.E. Evans, Phys. Plasmas 10 (2003) 3796;
T.E. Evans et al., Contrib. Plasma Phys. 44 (2004) 235.
[17] T.E. Evans, R.A. Moyer, P. Monat, Phys. Plasmas 9 (2002) 4957.
[18] A.M. Garofalo, R.J. La Haye, J.T. Scoville, Nucl. Fusion 42 (2002) 1335.
[19] T.E. Evans, R.A. Moyer, J. Nucl. Mater. 313–316 (2003) 1282.
[20] T.E. Evans, The ASDEX Team, Measurements of poloidal and toroidal energy deposition asymmetries in the ASDEX divertors, Max–Planck Institute for Plasma Physics Report IPP III/154, March 1991.
[21] P.H. Ghendrih, A. Grosman, H. Caps, Plasma Phys. Control. Fusion 38 (1996) 1653.